coatings

MDPI

Article

Effect of Electrochemically Deposited MgO Coating on Printable Perovskite Solar Cell Performance

T. A. Nirmal Peiris [1,2,*], Ajay K. Baranwal [2], Hiroyuki Kanda [2], Shouta Fukumoto [2], Shusaku Kanaya [2], Takeru Bessho [1], Ludmila Cojocaru [1], Tsutomu Miyasaka [3], Hiroshi Segawa [1,4] and Seigo Ito [2,*]

1 Research Center for Advanced Science and Technology (RCAST), The University of Tokyo, 4-6-1 Komaba, Meguro-ku, Tokyo 153-8904, Japan; t.bessho@dsc.rcast.u-tokyo.ac.jp (T.B.); cojocaru@dsc.rcast.u-tokyo.ac.jp (L.C.); csegawa@mail.ecc.u-tokyo.ac.jp (H.S.)

2 Department of Materials and Synchrotron Radiation Engineering, Graduate School of Engineering, University of Hyogo, 2167 Shosha, Hyogo, Himeji 671-2280, Japan; ajaybarn@gmail.com (A.K.B.); hiroyuki.k.8ch@gmail.com (H.K.); ej16t012@steng.u-hyogo.ac.jp (S.F.); mikan.ponkan.yuzu.hassaku@gmail.com (S.K.)

3 Graduate School of Engineering, Toin University of Yokohama, Kanagawa, Yokohama 225-8503, Japan; miyasaka@toin.ac.jp

4 Department of General Systems Studies, Graduate School of Arts and Science, The University of Tokyo, 3-8-1 Komaba, Meguro-ku, Tokyo 153-8902, Japan

* Correspondence: nirmalprs@gmail.com (T.A.N.P.); itou@eng.u-hyogo.ac.jp (S.I.); Tel.: +44-739-220-8971 (T.A.N.P.); +81-79-267-4150 (S.I.)

Academic Editor: I. M. Dharmadasa
Received: 5 January 2017; Accepted: 12 February 2017; Published: 27 February 2017

Abstract: Herein, we studied the effect of MgO coating thickness on the performance of printable perovskite solar cells (PSCs) by varying the electrodeposition time of $Mg(OH)_2$ on the fluorine-doped tin oxide (FTO)/TiO_2 electrode. Electrodeposited $Mg(OH)_2$ in the electrode was confirmed by energy dispersive X-ray (EDX) analysis and scanning electron microscopic (SEM) images. The performance of printable PSC structures on different deposition times of $Mg(OH)_2$ was evaluated on the basis of their photocurrent density-voltage characteristics. The overall results confirmed that the insulating MgO coating has an adverse effect on the photovoltaic performance of the solid state printable PSCs. However, a marginal improvement in the device efficiency was obtained for the device made with the 30 s electrodeposited TiO_2 electrode. We believe that this undesirable effect on the photovoltaic performance of the printable PSCs is due to the higher coverage of TiO_2 by the insulating MgO layer attained by the electrodeposition technique.

Keywords: MgO; $Mg(OH)_2$; electrodeposition; printable; perovskite; solar cells

1. Introduction

Perovskite solar cell (PSC) technology has made tremendous progress over the last few years, with a significant increase in power conversion efficiency with recent devices reaching over 22% [1]. Initially, perovskite ($CH_3NH_3PbI_3$) was used as a sensitizer to replace organic dye molecules in dye-sensitized solar cells by Miyasaka et al. [2]. However, corrosion of the $CH_3NH_3PbI_3$ by the I^-/I_3^- electrolyte hindered the interest of this new sensitizer until realizing the possibility of replacing the electrolyte with a solid organic hole transport material (HTM), spiro MeOTAD [3]. Since then, both mesoscopic and planar heterojunction PSCs have been fabricated with different architectures and preparation methods [4–7]. Recently, huge interest was given to printable PSCs with carbon counter electrodes as they demonstrate enormous potential for achieving high efficiency, long lifetime and low manufacturing costs which may lead to future commercialization [7–9].

In PSCs, often a thin compact TiO_2 layer (~50 nm) is formed in order to prevent back electron transport from fluorine-doped tin oxide (FTO) to either perovskite or HTM. However, unevenness, surface defects and the presence of pin holes in this layer are often responsible for reducing the cell performance. Therefore, over the last years, many attempts have been made to enhance the overall cell performance of PSCs by retarding the back transfer of photo-generated electrons through the FTO/TiO_2 interface by surface modification of TiO_2 using insulating metal oxides [10–12] and hydroxides [13,14] or high band gap semiconductors [15,16] that form a blocking layer between the perovskite sensitizer and TiO_2 layer to block the back electron flow towards the HTM. For instance, TiO_2 modification with a monolayer of silane [17] and ZnO with 3-aminopropanioc acid self-assembled monolayer [18] have been found to enhance the device efficiency by retarding the back electron transfer processes of PSCs. Wang et al. [19] found that magnesium oxide and magnesium hydroxide, formed at the surface of TiO_2, suppress the recombination, achieving an improvement of V_{oc} and hence photo-conversion efficiency (PCE). Similarly, Jung et al. [10] coat an ultrathin MgO layer on TiO_2 and found an improvement in the fill factor and V_{oc} of the device, which they believe to be due to the retarded charge recombination at the interface between MgO and $CH_3NH_3PbI_3$. Conversely, Ke et al. [20] and Liu et al. [21] have shown that a higher V_{oc} can be obtained for planar PSCs without a compact TiO_2 layer, suggesting that the recombination pathways in PSCs are still unclear and more investigation with different device configurations is required for better understanding.

Compared to other widely used coating techniques such as spin coating and screen printing, the electrodeposition is considered to be a versatile technique for producing surface coatings, owing to its precise controllability, better adherence to substrate, rapid deposition rate with a higher uniformity, room temperature operation and relatively low cost [22–24]. In this study, we grew a conformal $Mg(OH)_2$ coating by the electrodeposition method on the surface of FTO/TiO_2 and investigated the effect of this insulating oxide on their photovoltaic device performance. Our results confirmed that there is an adverse effect on the device performance with the MgO coating obtained by electrodeposition of $Mg(OH)_2$ on the printable PSCs.

2. Materials and Methods

Fluorine-doped tin oxide (FTO) glass substrates were etched with a laser before being cleaned ultrasonically with detergent, deionized water and ethanol successively. Then, some of the substrates were coated with a TiO_2 compact layer by aerosol spray pyrolysis at 500 °C using a precursor containing 300 µL of titanium diisopropoxide *bis* (acetylacetonate). The treated film was annealed at 500 °C for 30 min inside an oven. Then, the mesoporous TiO_2 layer was deposited by screen printing using a TiO_2 paste [3 g of F-6 powder (Showatitanium, Toyama, Japan) with 0.5 mL of acetic acid, 15 mL of ethyl cellulose (45–55 mPa·s, TCI, 10 wt % in EtOH) and 50 g of α-terpineol]. After the coating, the film was dried at 125 °C for 5 min and sintered at 500 °C for 30 min using an oven. The $Mg(OH)_2$ coatings were electrodeposited on the FTO/TiO_2 or FTO substrates in an aqueous electrolyte solution composed of $Mg(CH_3COO)_2{\cdot}4H_2O$ having a concentration of 0.01 M. The electrodeposition was carried out in the three-electrode configuration using the TiO_2-coated FTO or FTO substrate as the working electrode with the cathode area of 1 cm^2, Ag/AgCl electrode, and Pt as the reference and counter electrodes, respectively. The electrodeposition was conducted at a constant current of 0.6 mA (Chronopotentiometry) using a Potentiostat/Galvanostat. After the deposition, the films were removed from the electrolyte solution, washed with distilled water and allowed to dry at room temperature. The electrodeposition time was varied for 10 s, 30 s, 1 min, 2 min, 4 min, 6 min, 10 min and 20 min and the deposited $Mg(OH)_2$ is converted to MgO during the post-annealing of successive layers. In devices A and B, a ZrO_2 space layer was printed on the film using a ZrO_2 paste [3 g of ZrO_2 powder (40–50 nm, Alfa Aesar, Lancashire, UK) with 0.5 mL of acetic acid, 15 mL of ethyl cellulose (45–55 mPa·s, TCI, 10 wt % in EtOH) and 50 g of α-terpineol]. The film was annealed at 400 °C for 30 min inside an oven after drying at 125 °C for 5 min on a hot plate. Then, a NiO mesoporous layer was coated on respective devices using a NiO paste consisting of 3 g of NiO powder (20 nm,

Iolitec Ionic Liquids Technologies GmbH, Heilbronn, Germany) with 0.5 mL of acetic acid, 15 mL of ethyl cellulose (45–55 mPa·s, TCI, 10 wt % in EtOH) and 50 g of α-terpineol. After the pre-drying at 125 °C, the NiO layer was sintered at 500 °C for 30 min using an oven. Finally, a carbon black/graphite layer was coated on the top of the ZrO_2 or NiO layer by the screen printing method using a pot milled carbon black/graphite paste [1 g of Printex L6 carbon (Evonik Industries, Frankfurt, Germany), 1 g of graphite, 4 g of graphite flakes (~325 mesh, Alfa Aeser, Haverhill, MA, USA), 5 g of TiO_2 (P25), 20 g of α-terpineol and 30 g of ethyl cellulose (10 wt % in EtOH) and sintered at 400 °C for 30 min inside an oven. The synthesis of $CH_3NH_3PbI_3$ ($MAPbI_3$) and deposition on the devices was carried out by the two-step deposition method onto the carbon black/graphite layer (using 1.2 M PbI_2 in DMF solution and CH_3NH_3I solution (10 mg/mL)]. Upon drying at 70 °C for 30 min, the films darkened in colour, indicating the formation of $MAPbI_3$ in the solar cell. All of the processes were performed under ambient conditions.

Photovoltaic measurements were conducted using an AM 1.5 solar simulator equipped with a xenon lamp (Yamashita Denso, Tokyo, Japan). The power of the simulated light was calibrated to 100 $mW \cdot cm^{-2}$ by a reference Si photodiode (Bunkou Keiki, Tokyo, Japan). *J–V* curves were obtained by applying an external bias to the cell and the generated photocurrent was measured with a B2901A, Agilent voltage current source (Santa Clara, CA, USA). The active area of the cells was fixed at 0.04 cm^2. The SEM images were obtained by JOEL-JSM-6510 scanning electron microscopes (JEOL, Tokyo, Japan) and EDX measured using a TE3030, Hitachi machine (Tokyo, Japan).

3. Results and Discussion

In order to investigate the effect of MgO on the photovoltaic performance of printable PSCs, we have deposited a MgO layer on FTO/TiO_2 (devices B and C) or FTO (device D) by varying the $Mg(OH)_2$ electrodeposition time on different mesoscopic structures (Figure 1). The deposited $Mg(OH)_2$ is converted to MgO upon post-annealing of successive layers. The devices made with a standard four-layer structure of TiO_2/ZrO_2/NiO/Carbon ($MAPbI_3$) are depicted as A and the devices with the same architecture with MgO coating on TiO_2 are illustrated as device B. Device C is employed with the intention of fabricating a thin insulation layer of MgO on TiO_2 and FTO (with the deposition time) before coating the hole-transporting NiO layer. Device D is designed according to the meso-super-structured solar cell structure where the MgO layer is acting as a scaffold for $MAPbI_3$ in the device.

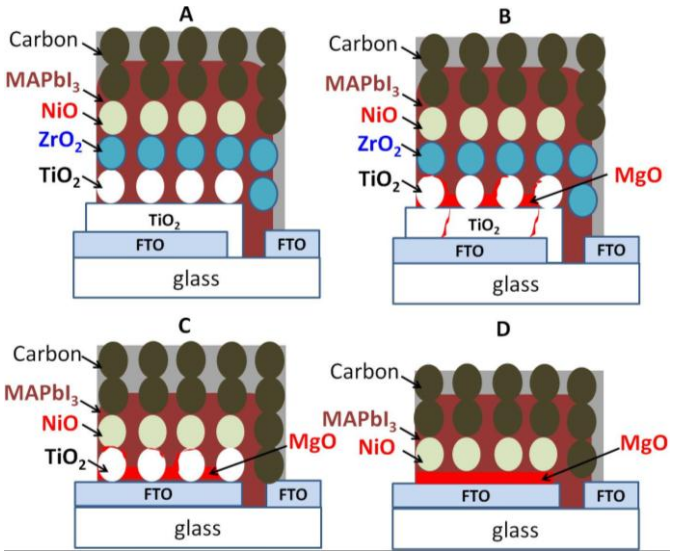

Figure 1. Different printable perovskite solar cell structures. (**A**) FTO/TiO_2/ZrO_2/NiO/Carbon ($MAPbI_3$); (**B**) FTO/TiO_2<MgO>/ZrO_2/NiO/Carbon ($MAPbI_3$); (**C**) FTO/TiO_2<MgO>/NiO/Carbon ($MAPbI_3$) and (**D**) FTO/MgO/NiO/Carbon ($MAPbI_3$).

During the electrodeposition of $Mg(OH)_2$ in the devices B, C and D, the below electrochemical reactions could take place at the cathode surface [13],

$$NO_3^- + H_2O + 2e^- \rightarrow NO_2^- + 2OH^- \quad (1)$$

$$2H_2O + 2e^- \rightarrow 2OH^- + H_2 \quad (2)$$

As a result of these reactions (i.e., with the formation of OH^-), a steep increase of local pH (~9) in the electrodeposition solution near to the cathode could occur, leading to the formation of $Mg(OH)_2$ due to the poor solubility of $Mg(OH)_2$ (K_{sp} of $Mg(OH)_2$ is 1.2×10^{-11} $mol^3 \cdot dm^{-9}$ at 25 °C) [25,26]. This flocculated $Mg(OH)_2$ in the solution can be hetero-coagulated on TiO_2 and FTO electrostatically due to their opposite surface charges. (Isoelectric points of TiO_2 ~6.2 FTO ~6 and $Mg(OH)_2$ ~12) [13]. Once the electrodeposition is started, it is more likely that the low resistive exposed FTO surface (i.e., pinholes) and the TiO_2 surface in the vicinity are coated with $Mg(OH)_2$. However, with the increasing deposition time, the alkaline pH boundary extends further away from the interior surface which could lead to the TiO_2 nanoparticles being covered by $Mg(OH)_2$.

The surface topographic FEG-SEM images of electrodeposited $Mg(OH)_2$ for 2 min and 10 min deposition times on FTO glass substrate are shown in Figure 2a,b respectively. The images showed that the substrates are completely covered by electrodeposited flower-like $Mg(OH)_2$ spheres [13,27]. Figure 2c,d shows the cross-sectional images of devices C and D respectively. As shown in Figure 2c, the thickness of the TiO_2<MgO>/ZrO_2/NiO ($MAPbI_3$) is around 2 µm whereas the carbon counter electrode is estimated to be around 25 µm. The MgO layer in the device cannot be seen clearly as it is too thin to be visible in the cross-sectional images. However, EDX (Figure 2e) mapping of the cross-sectional image of device D, confirms the presence of Mg, Ni and carbon in the electrode.

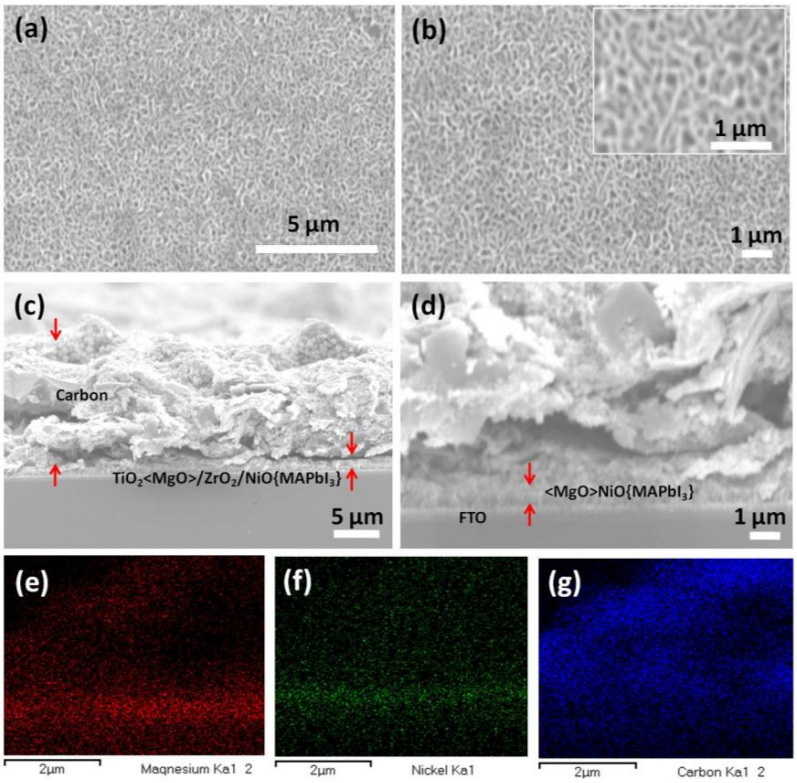

Figure 2. Surface topographical images of electrodeposited $Mg(OH)_2$ on the FTO substrate for (**a**) 2 min and (**b**) 10 min (inset shows the higher magnification), cross-sectional images of PSCs device B (**c**) and device D (**d**) and EDX mapping images of the MgO layer (**e**), NiO layer (**f**) and Carbon (**g**) in the device D.

The influence of the MgO layer and its thickness (by varying the $Mg(OH)_2$ electrodeposition time) on the photovoltaic performance of these different printable PSC structures was evaluated by their *I–V* characteristics. Figure 3 illustrates the variations observed in the *I–V* characteristics of the $TiO_2/ZrO_2/NiO/Carbon(MAPbI_3)$ structured device (device A) against the $Mg(OH)_2$ deposition time (device B). The device A yielded a V_{oc} of 0.78 V, a short-circuit current density (J_{sc}) of 9.30 mA·cm^{-2} and a fill factor of 0.44, which correspond to a PCE of 3.19%. The *I–V* plots and the average photovoltaic parameters in Table 1 of devices show that the device's performance is clearly influenced by the systematic growth of $Mg(OH)_2$ on TiO_2. The cell prepared with the 30 s $Mg(OH)_2$ electrodeposited electrode showed a V_{oc} of 0.75 V, J_{sc} of 8.48 mA·cm^{-2}, fill factor of 0.52 and PCE of 3.26%. It is noticeable that the J_{sc} has systematically decreased as the $Mg(OH)_2$ coating time varied from 1 to 10 min, suggesting the blocking of porous TiO_2. It is more likely that the coverage of $Mg(OH)_2$ on TiO_2 prevents $MAPbI_3$ on TiO_2 which was evident by the small reduction of photocurrent density up to 30 s. The trend was continued as the electrodeposition time further increased. The device with 10 min of $Mg(OH)_2$ coating showed the lowest J_{sc} of 0.61 mA·cm^{-2}, with a trivial improvement in the V_{oc} (0.79 V) and fill factor (0.53) compared to device A.

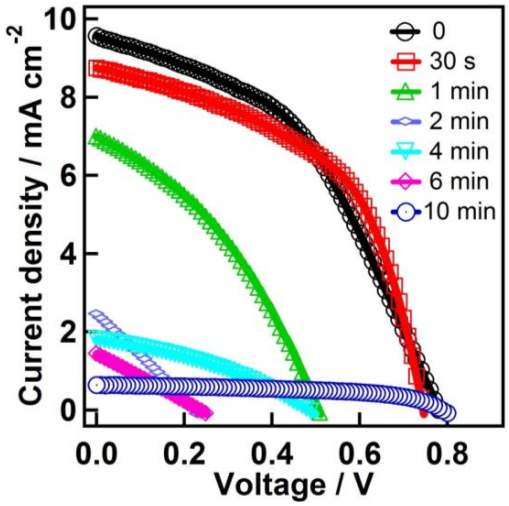

Figure 3. *J–V* characteristics of printable PSCs (device A) with different electrodeposition times of $Mg(OH)_2$ (device B).

Table 1. Summary of the average solar cell parameters of devices A and B against the electrodeposition times of $Mg(OH)_2$.

Time	J_{sc} (mA·cm^{-2})	V_{oc} (V)	Fill Factor	PCE (%)
0	9.30 ± 0.23	0.78 ± 0.01	0.44 ± 0.01	3.19 ± 0.14
30 s	8.48 ± 0.38	0.75 ± 0.01	0.52 ± 0.01	3.26 ± 0.15
1 min	6.32 ± 0.68	0.48 ± 0.04	0.36 ± 0.01	1.10 ± 0.20
2 min	2.26 ± 0.17	0.20 ± 0.02	0.26 ± 0.01	0.12 ± 0.02
4 min	1.69 ± 0.19	0.47 ± 0.03	0.34 ± 0.02	0.27 ± 0.06
6 min	1.32 ± 0.16	0.22 ± 0.03	0.26 ± 0.01	0.07 ± 0.02
10 min	0.61 ± 0.03	0.79 ± 0.01	0.53 ± 0.01	0.26 ± 0.01

In device C, $Mg(OH)_2$ was electrodeposited after coating the mesoporous TiO_2 layer without a compact TiO_2 layer and the MgO layer was replaced with TiO_2 and ZrO_2 layers in the device D. As shown in Figure 4a and Table 2, device C demonstrated poor device performance compared to the device A. This is probably due to the higher recombination rate at the TiO_2/NiO interface despite the MgO layer on TiO_2. The bare device demonstrated a J_{sc} of 4.99 mA·cm^{-2}, a V_{oc} of 0.10 V and a FF of 0.26, leading to a PCE of 0.14%.The device made with a coating of $Mg(OH)_2$ for 30 s on the FTO/TiO_2 electrode showed a PCE of 0.05%, with a significant decrease in both the J_{sc} (from 4.99

to 3.75 mA·cm^{-2}) and V_{oc} (from 0.10 to 0.06 V). Although an improvement in PCE was observed when the electrodeposition time increases from 2 to 4 min, the device efficiency is still inferior to the performance of the bare solar cell (Table 2).

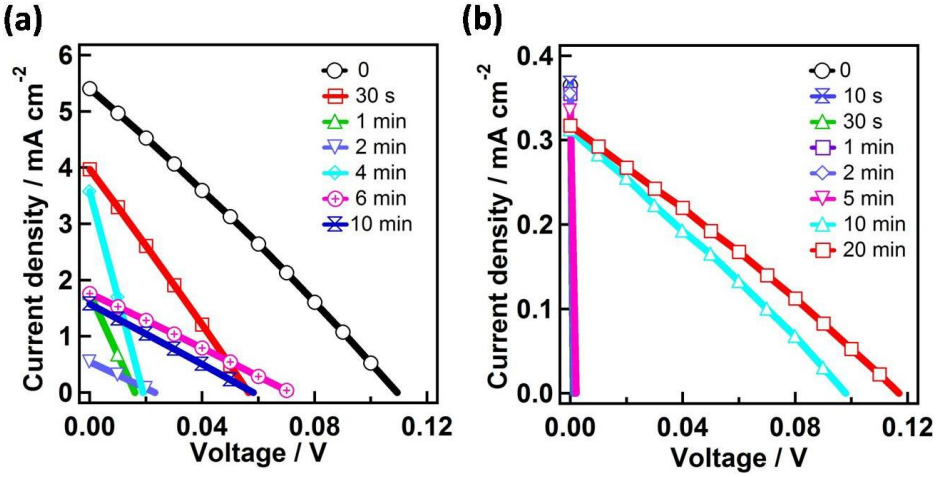

Figure 4. *J–V* characteristics of printable PSCs of device C (**a**) and device D (**b**) with different electrodeposition times of $Mg(OH)_2$.

Following the meso-super-structured solar cell proposed by Snaith et al. [3], we fabricated device D with FTO/$Mg(OH)_2$/NiO/Carbon($MAPbI_3$) configuration. In this structure, MgO acts as a scaffold for $MAPbI_3$. The *I–V* characteristics of the devices with different electrodeposition times of $Mg(OH)_2$ are shown in Figure 4b. It was clear that up to 10 min electrodeposition time of $Mg(OH)_2$, the diode characteristic did not appear due to the shorting resulted by the low thickness of the MgO layer. However, the diode characteristic emerged above the 10 min electrodeposition time of $Mg(OH)_2$. The device made with the 20 min deposited MgO layer showed a J_{sc} of 0.32 mA·cm^{-2}, a V_{oc} of 0.12 V, a fill factor of 0.27 and a PCE of 0.01% (Table 2). However, the higher thickness of MgO does not improve the photocurrent density of the device as expected, which could be due to the higher sheet resistance that results from the thick insulating MgO layer at the higher deposition times.

Overall, the results confirmed that the MgO coating on FTO/TiO_2 (devices B and C) or FTO (device D) in printable PSCs does not show much benefit in improving the PCE compared to the bare devices, which could be due to the higher coverage of TiO_2 by the insulating MgO layer attained by the electrodeposition of $Mg(OH)_2$.

Table 2. Summary of the average solar cell parameters of devices C and D against the electrodeposition time of $Mg(OH)_2$.

Time (min)	J_{sc} (mA·cm^{-2})	V_{oc} (V)	Fill Factor	PCE (%)
Device C				
0	4.99 ± 0.56	0.10 ± 0.01	0.26 ± 0.01	0.14 ± 0.03
0.5	3.75 ± 0.51	0.06 ± 0.01	0.26 ± 0.01	0.05 ± 0.01
1	1.67 ± 0.09	0.02 ± 0.01	0.25 ± 0.01	0.009 ± 0.002
2	0.53 ± 0.03	0.021 ± 0.002	0.25 ± 0.01	0.0029 ± 0.0002
4	3.45 ± 0.22	0.019 ± 0.002	0.243 ± 0.006	0.02 ± 0.01
6	1.74 ± 0.03	0.071 ± 0.001	0.26 ± 0.01	0.032 ± 0.001
10	1.55 ± 0.04	0.058 ± 0.001	0.251 ± 0.002	0.023 ± 0.001
Device D				
10	0.31 ± 0.01	0.097 ± 0.001	0.27 ± 0.01	0.0079 ± 0.0001
20	0.32 ± 0.01	0.12 ± 0.01	0.27 ± 0.01	0.0099 ± 0.0002

4. Conclusions

In summary, we studied the effect of MgO coating on the photovoltaic performance of printable PSCs. Electrodeposition of $Mg(OH)_2$ was conducted on the surface of mesoporous TiO_2 on FTO in devices A, B and C and FTO in device D. The effect of electrodeposition time on the performance of printable PSCs was evaluated on the basis of their key cell parameters. The overall results confirmed that the insulating MgO coating has an adverse effect on the photovoltaic performance of the solid state printable PSCs. We believe that this adverse effect on the photovoltaic performance of the printable PSCs is due to the higher coverage of TiO_2 by the insulating MgO layer attained by the electrodeposition of $Mg(OH)_2$.

Acknowledgments: The authors would like to express sincere thanks to the New Energy and Industrial Technology Development Organization (NEDO).

Author Contributions: T.A. Nirmal Peiris and Seigo Ito designed the experiments. T.A. Nirmal Peiris and Ajay K. Baranwal performed the experiments. T.A. Nirmal Peiris, Hiroyuki Kanda, Shouta Fukumoto and Shusaku Kanaya analyzed the data. Takeru Bessho, Ludmila Cojocaru, Tsutomu Miyasaka, Hiroshi Segawa and Seigo Ito equally contributed in useful discussions and modifications. T.A. Nirmal Peiris wrote the paper.

Conflicts of Interest: The authors declare no conflict of interest.

References

1. NREL Best Research-Cell Efficiencies. Available online: http://www.nrel.gov/pv/assets/images/efficiency_chart.jpg (accessed on 15 December 2016).
2. Kojima, A.; Teshima, K.; Shirai, Y.; Miyasaka, T. Organometal Halide Perovskites as Visible-Light Sensitizers for Photovoltaic Cells. *J. Am. Chem. Soc.* **2009**, *131*, 6050–6051. [CrossRef] [PubMed]
3. Lee, M.M.; Teuscher, J.; Miyasaka, T.; Murakami, T.N.; Snaith, H.J. Efficient hybrid solar cells based on meso-superstructured organometal halide perovskites. *Science* **2012**, *338*, 643–647. [CrossRef] [PubMed]
4. Jeng, J.Y.; Chen, K.C.; Chiang, T.Y.; Lin, P.Y.; Tsai, T.D.; Chang, Y.C.; Guo, T.F.; Chen, P.; Wen, T.C.; Hsu, Y.J. Nickel oxide electrode interlayer in $CH_3NH_3PbI_3$ perovskite/PCBM planar-heterojunction hybrid solar cells. *Adv. Mater.* **2014**, *26*, 4107–4113. [CrossRef] [PubMed]
5. Qin, P.; Tanaka, S.; Ito, S.; Tetreault, N.; Manabe, K.; Nishino, H.; Nazeeruddin, M.K.; Tzel, M.G.A.; Grätzel, M. Inorganic hole conductor-based lead halide perovskite solar cells with 12.4% conversion efficiency. *Nat. Commun.* **2014**, *5*, 1–6. [CrossRef] [PubMed]
6. Mei, A.; Li, X.; Liu, L.; Ku, Z.; Liu, T.; Rong, Y.; Xu, M.; Hu, M.; Chen, J.; Yang, Y.; et al. A hole-conductor–free, fully printable mesoscopic perovskite solar cell with high stability. *Science* **2014**, *345*, 295–298. [CrossRef] [PubMed]
7. Baranwal, A.K.; Kanaya, S.; Peiris, T.A.N.; Mizuta, G.; Nishina, T.; Kanda, H.; Miyasaka, T.; Segawa, H.; Ito, S. 100 °C Thermal Stability of Printable Perovskite Solar Cells Using Porous Carbon Counter Electrodes. *ChemSusChem* **2016**, *9*, 2604–2608. [CrossRef] [PubMed]
8. Guo, D.; Yu, J.; Fan, K.; Zou, H.; He, B. Nanosheet-based printable perovskite solar cells. *Sol. Energy Mater. Sol. Cells* **2017**, *159*, 518–525. [CrossRef]
9. Park, N.-G.; Grätzel, M.; Miyasaka, T.; Zhu, K.; Emery, K. Towards stable and commercially available perovskite solar cells. *Nat. Energy* **2016**, *1*, 16152. [CrossRef]
10. Han, G.S.; Chung, H.S.; Kim, B.J.; Kim, D.H.; Lee, J.W.; Swain, B.S.; Mahmood, K.; Yoo, J.S.; Park, N.-G.; Lee, J.H.; et al. Retarding charge recombination in perovskite solar cells using ultrathin MgO-coated TiO_2 nanoparticulate films. *J. Mater. Chem. A* **2015**, *3*, 9160–9164. [CrossRef]
11. Kulkarni, A.; Jena, A.K.; Chen, H.W.; Sanehira, Y.; Ikegami, M.; Miyasaka, T. Revealing and reducing the possible recombination loss within TiO_2 compact layer by incorporating MgO layer in perovskite solar cells. *Sol. Energy* **2016**, *136*, 379–384. [CrossRef]
12. Ball, J.M.; Lee, M.M.; Hey, A.; Snaith, H.J. Low-temperature processed meso-superstructured to thin-film perovskite solar cells. *Energy Environ. Sci.* **2013**, *6*, 1739–1743. [CrossRef]
13. Peiris, T.A.N.; Senthilarasu, S.; Wijayantha, K.G.U. Enhanced Performance of Flexible Dye-Sensitized Solar Cells: Electrodeposition of $Mg(OH)_2$ on a Nanocrystalline TiO_2 Electrode. *J. Phys. Chem. C* **2012**, *116*, 1211–1218. [CrossRef]

14. Peiris, T.A.N.; Wijayantha, K.G.U.; García-Cañadas, J. Insights into mechanical compression and the enhancement in performance by $Mg(OH)_2$ coating in flexible dye sensitized solar cells. *Phys. Chem. Chem. Phys.* **2014**, *16*, 2912–2919. [CrossRef] [PubMed]
15. Taguchi, T.; Zhang, X.; Sutanto, I.; Tokuhiro, K.; Rao, T.N. Improving the performance of solid-state dye-sensitized solar cell using MgO-coated TiO_2 nanoporous film. *Chem. Commun* **2003**, 2480–2481. [CrossRef]
16. Lee, S.; Kim, J.Y.; Hong, K.S.; Jung, H.S.; Lee, J.K.; Shin, H. Enhancement of the photoelectric performance of dye-sensitized solar cells by using a $CaCO_3$-coated TiO_2 nanoparticle film as an electrode. *Sol. Energy Mater. Sol. Cells* **2006**, *90*, 2405–2412. [CrossRef]
17. Liu, L.; Mei, A.; Liu, T.; Jiang, P.; Sheng, Y.; Zhang, L.; Han, H. Fully Printable Mesoscopic Perovskite Solar Cells with Organic Silane Self-Assembled Monolayer. *J. Am. Chem. Soc.* **2015**, *137*, 1790–1793. [CrossRef] [PubMed]
18. Zuo, L.; Gu, Z.; Ye, T.; Fu, W.; Wu, G.; Li, H.; Chen, H. Enhanced photovoltaic performance of $CH_3NH_3PbI_3$ perovskite solar cells through interfacial engineering using self-assembling monolayer. *J. Am. Chem. Soc.* **2015**, *137*, 2674–2679. [CrossRef] [PubMed]
19. Wang, J.; Qin, M.; Tao, H.; Ke, W.; Chen, Z.; Wan, J.; Qin, P.; Xiong, L.; Lei, H.; Yu, H.; et al. Performance enhancement of perovskite solar cells with Mg-doped TiO_2 compact film as the hole-blocking layer. *Appl. Phys. Lett.* **2015**, *106*, 121104. [CrossRef]
20. Ke, W.; Fang, G.; Wan, J.; Tao, H.; Liu, Q.; Xiong, L.; Qin, P.; Wang, J.; Lei, H.; Yang, G.; et al. Efficient hole-blocking layer-free planar halide perovskite thin-film solar cells. *Nat. Commun.* **2015**, *6*, 6700. [CrossRef] [PubMed]
21. Liu, D.; Yang, J.; Kelly, T.L. Compact layer free perovskite solar cells with 13.5% efficiency. *J. Am. Chem. Soc.* **2014**, *136*, 17116–17122. [CrossRef] [PubMed]
22. Hernandez, S.; Ottone, C.; Varetti, S.; Fontana, M.; Pugliese, D.; Saracco, G.; Bonelli, B.; Armandi, M. Spin-coated vs. electrodeposited Mn oxide films as water oxidation catalysts. *Materials* **2016**, *9*, 296. [CrossRef]
23. Dharmadasa, I.M.; Haigh, J. Strengths and Advantages of Electrodeposition as a Semiconductor Growth Technique for Applications in Macroelectronic Devices. *J. Electrochem. Soc.* **2006**, *153*, G47–G52. [CrossRef]
24. Wessels, K.; Minnermann, M.; Rathousky, J.; Wark, M.; Oekermann, T. Influence of Calcination Temperature on the Photoelectrochemical and Photocatalytic Properties of Porous TiO_2 Films Electrodeposited from Ti(IV)-Alkoxide Solution. *J. Phys. Chem. C* **2008**, *112*, 15122–15128. [CrossRef]
25. Zou, G.; Liu, R.; Chen, W. Highly textural lamellar mesostructured magnesium hydroxide via a cathodic electrodeposition process. *Mater. Lett.* **2007**, *61*, 1990–1993. [CrossRef]
26. Lv, Y.; Zhang, Z.; Lai, Y.; Li, J.; Liu, Y. Formation mechanism for planes (011) and (001) oriented $Mg(OH)_2$ films electrodeposited on SnO_2 coating glass. *CrystEngComm* **2011**, *13*, 3848–3851. [CrossRef]
27. Liu, M.; Wang, Y.; Chen, L.; Zhang, Y.; Lin, Z. $Mg(OH)_2$ supported nanoscale zero valent iron enhancing the removal of Pb(II) from aqueous solution. *ACS Appl. Mater. Interfaces* **2015**, *7*, 7961–7969. [CrossRef] [PubMed]